

Analytical and numerical investigation of heat and mass transfer effects on magnetohydrodynamic natural convective flow past a vertical porous plate

Rallabandi Srinivasa Raju^{a*}, Gampa Anitha^a and Gurejala Jithender Reddy^b

^aDepartment of Engineering Mathematics, GITAM University, Hyderabad, 502329, Medak (Dt), Telangana State, India

^bDepartment of Mathematics, VNR Vignana Jyothi Institute of Engineering and Technology, Hyderabad, Ranga Reddy (Dt), 500090, Telangana State, India.

PAPER INFO

History:

Submitted 2017-01-07

Revised 2017-07-25

Accepted 2017-03-03

Keywords:

Heat and Mass transfer;
Natural convection;
Hall current;
Porous medium;
Finite element method;
Perturbation technique

ABSTRACT

This study investigated the effects of the Hall current on the unsteady natural convective flow of a viscous, incompressible, and electrically conducting optically thick radiating fluid past a vertical porous plate in the presence of a uniform transverse magnetic field. Rosseland diffusion approximation was used to describe the radiative heat flux in the energy equation. Analytical and numerical solutions of coupled governing partial differential equations for fluid velocity, fluid temperature, and fluid concentration profiles were obtained via perturbation and finite element techniques, respectively. Graphs were used as bases for examining the effects of various dimensionless engineering parameters, namely, the Grashof number for heat and mass transfer, a magnetic field parameter, the Prandtl and Schmidt numbers, a thermal radiation parameter, the Hall parameter entering into the problem of primary and secondary velocities, and temperature and concentration profiles throughout the boundary layer. Expressions for skin friction, the Nusselt number, and the Sherwood number were derived and represented in tabular form. Results revealed that flow field and temperature distribution are considerably influenced by the thermal radiation parameter. The research also obtained limiting cases, which were found to be in good agreement with previously published results.

© 2017 Published by Semnan University Press. All rights reserved.

DOI: 10.22075/jhmtr.2017.1503.1100

1. Introduction

The natural convective flow induced by thermal and solutal buoyancy forces that act on bodies with different geometries in a fluid-saturated porous medium is prevalent in many natural phenomena and has wide-ranging industrial applications. In atmospheric flows, for example, maintaining the purity of air or water is impossible because foreign mass may be present either naturally or in mixed form with air or water due to industrial emissions. Natural processes such as the attenuation of toxic waste in water bodies, the vaporization of mist and fog, photosynthesis, the drying of porous solids, transpiration, sea wind formation (wherein upward

convection is modified by Coriolis forces), and ocean current formation occur because of the thermal and solutal buoyancy forces that develop as a result of temperature difference, temperature concentration, or a combination of these two. Such forces are also encountered in several practical systems for industry-based applications, including heat exchanger devices, molten metals (for cooling), insulation systems, petroleum reservoirs, filtration systems, chemical catalytic reactors and processes, nuclear waste repositories, desert coolers, wet bulb thermometers, and frost formation in vertical channels.

Considering the importance of the above-mentioned fluid flow problems, extensive research has been carried out on these issues. Raju et al. [1], for instance, derived analytical and numerical

Corresponding Author : Department of Engineering Mathematics,
GITAM University, Hyderabad, 502329, Medak (Dt), Telangana
State, India
Email : srivass999@gmail.com

solutions of unsteady magnetohydrodynamic (MHD) free convective flow over an exponentially moving vertical plate with heat absorption. Reddy and Raju [2] studied transient MHD free convective flow past an infinite vertical plate embedded in a porous medium with viscous dissipation. Raju et al. [3] probed into the application of the finite element method in the examination of unsteady MHD free convective flow past a vertically inclined porous plate. The authors included thermal diffusion and diffusion thermo effects in their analysis. Similarly, Raju et al. [4] used the finite element method to illuminate thermal diffusion and diffusion thermo effects on unsteady heat and mass transfer MHD natural convective Couette flow. Murthy et al. [5] studied heat and mass transfer effects on MHD natural convective flow past an infinite vertical porous plate in the presence of thermal radiation and the Hall current. Sivaiah and Raju [6] investigated finite element solutions of heat and mass transfer flow on the basis of the Hall current, heat sources, and viscous dissipation. Rao et al. [7] also examined finite element solutions of heat and mass transfer, this time with particular concentration on the MHD flow of a viscous fluid past a vertical plate under oscillatory suction velocity. Rao et al. [8] discussed chemical reaction effects on unsteady MHD free convective fluid flow past a semi-infinite vertical plate embedded in a porous medium with heat absorption. The combined influence of thermal diffusion and diffusion thermo on chemical reacted magnetohydrodynamic free convection from an impulsively started infinite vertical plate embedded in a porous medium studied by Jithender Reddy et al. [9] using finite element method. Ramya et al. [10] discussed the influence of chemical reaction on the MHD boundary layer flow of nanofluids over a nonlinearly stretching sheet with thermal radiation. Ramya et al. [11] studied the slip effect of the MHD boundary layer flow of nanofluid particles over a non-linearly isothermal stretching sheet in the presence of heat generation/absorption. Applying the finite element method, Rao et al. [12] obtained numerical solutions to MHD transient flow past an impulsively started infinite horizontal porous plate in a rotating fluid with the Hall current. Radiation and mass transfer flow past a semi-infinite moving vertical plate with viscous dissipation was examined via finite element analysis by Rao et al. [13]. The combined influence of thermal diffusion and diffusion thermo effects on unsteady hydromagnetic free convective fluid flow past an infinite vertical porous plate in the presence of chemical reaction was investigated by Raju et al. [14]. The effects of thermal radiation and heat source on unsteady MHD free convective flow past an infinite vertical plate with thermal diffusion and diffusion thermo effects were studied by Raju et al. [15]. The effects of a magnetic field on the flow field, heat transfer, and entropy generation of Cu–water nanofluid mixed

convection in a trapezoidal enclosure were investigated by Aghaei et al. [16]. Aghaei et al. [17] studied the effects of a magnetic field on the flow field and heat transfer of nanofluid with variable properties in a square enclosure with two heat sources.

The study of many transport processes existing in nature and in industrial applications, wherein heat and mass transfer is a consequence of buoyancy effects caused by the diffusion of heat and chemical species, is useful for improving a number of chemical technologies, such as polymer production, enhanced oil recovery, underground energy transport, ceramic manufacturing, and food processing. Heat and mass transfer from different geometries embedded in porous media finds numerous engineering and geophysical applications. For example, it is considered in the drying of porous solids, the use of thermal insulation, and the cooling of nuclear reactors. At high operating temperatures, radiation effects can be significant. Because many engineering processes are implemented at high temperatures, knowledge of radiation heat transfer is critical in the design of reliable equipment, nuclear plants, gas turbines, and various propulsion devices or aircraft, missiles, satellites, and space vehicles. The combination of heat and mass transfer problems with chemical reaction is equally important in many processes and has therefore received considerable attention in recent years. Such combination has found numerous applications in, for example, the design of chemical processing equipment, investigations of crop damage due to freezing, and the use of food processing and cooling towers. In this regard, Deka et al. [18] investigated the effects of first-order homogeneous chemical reaction on unsteady flow past an infinite vertical plate with constant heat and mass transfer. Muthucumaraswamy and Ganesan [19] discussed the effects of chemical reaction and injection on the flow characteristics of the unsteady upward motion of an isothermal plate. The MHD flow of a uniformly stretched vertical permeable surface in the presence of heat generation/absorption and chemical reaction was considered by Chamkha [20]. Ibrahim et al. [21] obtained an analytical solution for unsteady MHD free convective flow past a semi-infinite vertical permeable moving plate with a heat source and chemical reaction. Rahman et al. [22] studied heat transfer in micropolar fluid with temperature-dependent fluid properties along a non-stretching sheet.

Despite the insights provided by the aforementioned studies, none of them explained the effects of thermal radiation on flow and heat transfer. The effects of radiation on MHD flow and heat transfer problems have become increasingly important in industry given the previously stated issue of significant radiation at high operating temperatures, in which many engineering processes occur. The deficiency of the above-mentioned studies

in exploring radiation was addressed by other scholars. Cogley et al. [23], for example, showed that in an optically thin limit for a non-gray gas near equilibrium, the fluid does not absorb its own emitted radiation but absorbs the radiation emitted by boundaries. Satter and Hamid [24] investigated unsteady free convective interaction with thermal radiation in boundary layer flow past a vertical porous plate. Vajravelu [25] shed light on the flow of a steady viscous fluid and heat transfer characteristics in a porous medium by considering different heating processes. Hossain and Takhar [26] considered radiation effects on the mixed convective boundary layer flow of an optically dense viscous incompressible fluid along a vertical plate with uniform surface temperature. Raptis [27] investigated the steady flow of a viscous fluid through a porous medium bounded by a porous plate subjected to a constant suction velocity through the presence of thermal radiation. Makinde [28] examined transient free convective interaction with the thermal radiation of an absorbing emitting fluid along a moving vertical permeable plate. The effects of chemical reaction and radiation absorption on unsteady MHD free convective flow past a semi-infinite vertical permeable moving plate with a heat source and suction was studied by Ibrahim et al. [29]. Bakr [30] presented an analysis of MHD free convection and mass transfer adjacent to a moving vertical plate for micropolar fluid in a rotating frame of reference under the presence of heat generation/ absorption and a chemical reaction.

When the density of an electrically conducting fluid is low and/or when an applied magnetic field is strong, the Hall current is produced in the flow field. The Hall current plays an important role in determining the features of flow problems because it induces secondary flow in the flow field. With this consideration in mind, several researchers comprehensively investigated hydromagnetic free convective flow past a flat plate with Hall effects under different thermal conditions. Some of these works are those conducted by Pop and Watanabe [31], Abo-Eldahab and Elbarbary [32], Takhar et al. [33], and Saha et al. [34]. Note that the Hall current's inducement of secondary flow in the flow field resembles the characteristics of Coriolis force. Comparing the individual effects of these two phenomena and their combined influence on fluid flow problems is therefore a crucial component of fluid flow research. Such effort has been initiated by certain studies, such as that of Narayana et al. [35], who probed into the effects of the Hall current and radiation-absorption on the MHD natural convective heat and mass transfer flow of a micropolar fluid in a rotating frame of reference. Seth et al. [36] investigated the effects of the Hall current and rotation on the unsteady hydromagnetic natural convective flow of a viscous, incompressible, electrically conducting, and heat-absorbing fluid past

an impulsively moving vertical plate with ramped temperature in a porous medium. The authors also took the effects of thermal diffusion into account.

The main purpose of the present investigation was to illuminate the effects of the Hall current and thermal radiation on unsteady MHD natural convective heat and mass transfer flow past a vertical porous plate. We assumed that the plate is embedded in a uniform porous medium and oscillates in time with a constant frequency in the presence of a transverse magnetic field. Governing equations were solved numerically using the finite element technique, and numerical results were derived for various values of the physical parameters of interest.

2. Mathematical formulations

The fundamental equations that govern the motion of an incompressible, viscous, and electrically conducting fluid in the presence of a magnetic field are as follows [37]:

Equation of continuity:

$$\nabla \cdot \bar{v} = 0 \quad (1)$$

Momentum equation:

$$\rho \left[\frac{\partial \bar{v}}{\partial t'} + (\bar{v} \cdot \nabla) \bar{v} \right] = -\nabla P + \bar{J} \times \bar{B} + \rho \bar{g} + \mu \nabla^2 \bar{v} - \frac{\mu}{k'} \bar{v} \quad (2)$$

Energy equation:

$$\rho C_p \left[\frac{\partial T'}{\partial t'} + (\bar{v} \cdot \nabla) T' \right] = \kappa \nabla^2 T' - \frac{\partial q_r}{\partial y'} \quad (3)$$

Species continuity equation:

$$\frac{\partial C'}{\partial t'} + (\bar{v} \cdot \nabla) C' = D \nabla^2 C' \quad (4)$$

Kirchhoff's first law:

$$\nabla \cdot \bar{J} = 0 \quad (5)$$

General Ohm's law, with consideration for Hall effects:

$$\bar{J} + \frac{\omega_e \tau_e}{B_0} (\bar{J} \times \bar{B}) = \sigma \left(\bar{E} + \bar{v} \times \bar{B} + \frac{1}{e \eta_e} \nabla p_e \right) \quad (6)$$

Gauss's law of magnetism:

$$\bar{\nabla} \cdot \bar{B} = 0 \quad (7)$$

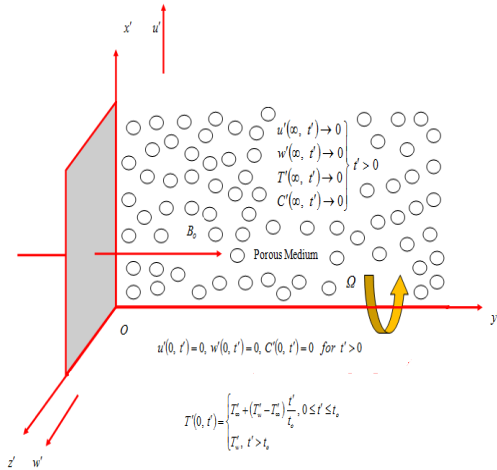


Fig. 1. Geometry of the problem

The unsteady flow of an electrically conducting fluid past an infinite vertical porous flat plate that coincides with the x' -axis $y' = 0$ was considered. For this case, thermal diffusion, the Hall current, and heat sources in the presence of a uniform transverse magnetic field were also taken into account. Our investigation was underlain by the following assumptions:

- i. The coordinate system is chosen in such a way that the x' -axis runs along the plate in an upward direction, and the y' -axis runs normal to the plane of the plate immersed in the fluid.
- ii. A uniform transverse magnetic field B_0 is applied in a direction parallel to the y' -axis.
- iii. Initially (i.e., at time $t' \leq 0$), both the fluid and plate are at rest and have uniform temperature T_∞' . Species concentration on the surface of the plate and at every point within the fluid is maintained at uniform concentration C_∞' .
- iv. The temperature at the surface of the plate is increased to uniform temperature T_w' , and species concentration on such surface is raised to uniform species concentration C_w' and maintained at this level thereafter.
- v. Given that the plate is of infinite extent in the x' direction and is electrically non-conducting, all physical quantities, except pressure, depend only on y' and t' .
- vi. No applied or polarized voltages exist, thereby rendering the effects of fluid polarization negligible. This corresponds to a case wherein no energy is incorporated into or extracted from fluid by electrical means [38].
- vii. The magnetic field induced by fluid motion is negligible in comparison to the applied magnetic field. This assumption is justified because the magnetic Reynolds number is very small for the

liquid metals and partially ionized fluids that are commonly used in industrial applications [38].
viii. No voltage is applied, suggesting the absence of an electric field.

ix. All the fluid properties, except density in the buoyancy force terms, are constant.

We introduce a coordinate system (x', y', z') , in which the x' -axis is positioned vertically upwards, the y' -axis is normal to the plate directed into the fluid region, and the z' -axis runs along the width of the plate. Let $\vec{v} = u'\hat{i} + v'\hat{j} + w'\hat{k}$ be the velocity, $\vec{J} = J_x\hat{i} + J_y\hat{j} + J_z\hat{k}$ be the current density at point $p(x', y', z', t')$, and $\vec{B} = B_0\hat{j}$ be the applied magnetic field, with $\hat{i}, \hat{j}, \hat{k}$ being the unit vectors along the x' -axis, y' -axis, and z' -axis, respectively. Because the plate is of infinite length in the x' and z' directions, all values, except perhaps that of pressure, are independent of x' and z' . Eq. (1) yields

$$\frac{\partial \vec{v}}{\partial y'} = 0 \tag{8}$$

which is trivially satisfied by

$$\vec{v} = -V_0 \tag{9}$$

where V_0 is a constant, and $V_0 > 0$. Therefore, velocity vector \vec{v} is obtained using

$$\vec{v} = u'\hat{i} - V_0\hat{j} + w'\hat{k} \tag{10}$$

Eq. (7) is satisfied by

$$\vec{B} = B_0\hat{j} \tag{11}$$

Eq. (5) is reduced to

$$\frac{\partial J_y}{\partial y'} = 0 \tag{12}$$

which shows that $J_y = \text{constant}$. Given that the plate is non-conducting, $J_y = 0$ at the plate and, hence, $J_y = 0$ at all points in the fluid. Accordingly, the current density is given by

$$\vec{J} = J_x\hat{i} + J_z\hat{k} \tag{13}$$

Under assumptions (iv) and (v), Eq. (6) takes the form

$$\bar{J} + \frac{m}{B_0} (\bar{J} \times \bar{B}) = \sigma (\bar{v} \times \bar{B}) \tag{14}$$

where $m = \omega_e \tau_e$ is the Hall parameter. Eqs. (10), (11), (13), and (14) yield

$$J_x = \frac{\sigma B_0}{1+m^2} (mu' - w') \tag{15}$$

and $J_z = \frac{\sigma B_0}{1+m^2} (u' + mw')$

With the above assumptions the usual boundary layer, and Boussinesq's approximation, Eqs. (2) to (4) are reduce to the following forms:

$$\begin{aligned} \frac{\partial u'}{\partial t'} + \nu \frac{\partial u'}{\partial y'} &= \nu \frac{\partial^2 u'}{\partial y'^2} - \frac{1}{(1+m^2)} \left[\frac{\sigma B_0^2}{\rho} \right] u' + \\ &\frac{m \sigma B_0^2}{\rho(1+m^2)} w' - \left[\frac{\nu}{k'} \right] u' + g\beta(T' - T'_\infty) \tag{16} \\ &+ g\beta^*(C' - C'_\infty) \end{aligned}$$

$$\begin{aligned} \frac{\partial w'}{\partial t'} + \nu \frac{\partial w'}{\partial y'} &= \nu \frac{\partial^2 w'}{\partial y'^2} + \frac{\sigma B_0^2 (mu' - w')}{\rho(1+m^2)} \tag{17} \\ &- \frac{\nu w'}{k'} \\ \frac{\partial(T' - T'_\infty)}{\partial t'} + \nu \frac{\partial(T' - T'_\infty)}{\partial y'} &= \frac{\kappa}{\rho C_p} \frac{\partial^2(T' - T'_\infty)}{\partial y'^2} \tag{18} \end{aligned}$$

$$\begin{aligned} &- \frac{1}{\rho C_p} \left(\frac{\partial q_r}{\partial y'} \right) \\ \frac{\partial(C' - C'_\infty)}{\partial t'} + \nu \frac{\partial(C' - C'_\infty)}{\partial y'} &= D \frac{\partial^2(C' - C'_\infty)}{\partial y'^2} \tag{19} \end{aligned}$$

For an optically thick fluid, both emission and self-absorption exist, and the absorption coefficient is usually wavelength dependent and large. These features enable the use of Rosseland approximation for the radiative heat flux vector. Thermal radiation is assumed present in the form of a unidirectional flux in the y' -direction, that is, q_r (transverse to the vertical surface). Using the Rosseland approximation [39], radiative heat flux q_r is derived thus:

$$q_r = - \left(\frac{4\sigma_s}{3k_e} \right) \frac{\partial T'^4}{\partial y'} \tag{20}$$

where σ_s is the Stefan–Boltzmann constant, and k_e denotes the mean absorption coefficient. Note that the adoption of Rosseland approximation limited the

present analysis to optically thick fluids. If temperature differences within flow are sufficiently small, then Eq. (20) can be linearized by expanding T'^4 in the Taylor series about T'_∞ , which, after disregarding higher-order terms, takes the following form:

$$T'^4 \cong T_\infty'^4 + 4(T' - T'_\infty)T_\infty'^3 = 4T'T_\infty'^3 - 3T_\infty'^4 \tag{21}$$

Using Eqs. (21) and (20) in the last term of Eq. (18) derives

$$\frac{\partial q_r}{\partial y'} = - \frac{16\sigma_s T_\infty'^3}{3k_e} \frac{\partial^2 T'}{\partial y'^2} \tag{22}$$

Introducing Eq. (22) into Eq. (18) produces the energy equation in the following form:

$$\begin{aligned} \frac{\partial(T' - T'_\infty)}{\partial t'} + \nu \frac{\partial(T' - T'_\infty)}{\partial y'} &= \left(\frac{\kappa}{\rho C_p} \right) \frac{\partial^2 T'}{\partial y'^2} \tag{23} \\ &+ \left(\frac{16\sigma_s T_\infty'^3}{3k_e \rho C_p} \right) \frac{\partial^2 T'}{\partial y'^2} \end{aligned}$$

In Eq. (18), viscous dissipation and Ohmic dissipation are disregarded, and in Eq. (19), the term arising from chemical reaction is absent. We now use $\nu = -V_0, T'(y', t') - T'_\infty = \theta(y', t')$ and $C'(y', t') - C'_\infty = \phi(y', t')$ subject to boundary conditions

$$t' \leq 0 : u' = 0, w' = 0, T' = T'_\infty, C' = C'_\infty \text{ for all } y'$$

$$t' \leq t_o : T' = T'_\infty + (T'_w - T'_\infty) \frac{t'}{t_o} \text{ at } y' = 0$$

$$\begin{aligned} t' > 0 : &\left\{ \begin{aligned} &u' = 0, w' = 0, \\ &T' = T'_\infty + (T'_w - T'_\infty) \frac{t'}{t_o}, \\ &C' = C'_w \text{ at } y' = 0 \\ &u' \rightarrow 0, w' \rightarrow 0, T' \rightarrow T'_\infty, \\ &C' \rightarrow C'_\infty \text{ as } y' \rightarrow \infty \end{aligned} \right. \\ t' > t_o : &\left\{ \begin{aligned} &T' = T'_w \text{ at } y' = 0 \\ &T' \rightarrow T'_\infty \text{ as } y' \rightarrow \infty \end{aligned} \right. \tag{24} \end{aligned}$$

Characteristic time t_o is defined according to the non-dimensional process mentioned above as

$t_o = \frac{\nu}{V_0}$. Let us introduce the following dimensionless quantities:

$$\left. \begin{aligned} \eta &= \frac{V_0 y'}{\nu}, t = \frac{V_0^2 t'}{4\nu}, u = \frac{u'}{V_0}, w = \frac{w'}{V_0}, \\ \phi &= \frac{C'}{b}, Gr = \frac{4g\beta va}{V_0^3}, Gc = \frac{4g\beta^* vb}{V_0^3}, \\ M &= \frac{4B_0^2 \sigma \nu}{\rho V_0^3}, Pr = \frac{\nu \rho C_p}{\kappa}, Sc = \frac{\nu}{D}, \\ K &= \frac{V_0^2 k'}{4\nu^2}, F = \frac{4\sigma_s T_\infty^3}{k_e \kappa}, \theta = \frac{\theta'}{a} \end{aligned} \right\} \quad (25)$$

Eqs. (16) to (19) are converted into the following non-dimensional forms, respectively:

$$\frac{\partial u}{\partial t} - 4 \frac{\partial u}{\partial \eta} = 4 \frac{\partial^2 u}{\partial \eta^2} - \frac{M}{(1+m^2)}(u+mw) \quad (26)$$

$$+ Gr\theta + Gc\phi - \frac{u}{K} \quad (27)$$

$$\frac{\partial w}{\partial t} - 4 \frac{\partial w}{\partial \eta} = 4 \frac{\partial^2 w}{\partial \eta^2} - \frac{M}{(1+m^2)}(mu-w) - \frac{w}{K} \quad (27)$$

$$\frac{\partial \theta}{\partial t} - 4 \frac{\partial \theta}{\partial \eta} = \frac{4}{Pr} \left(1 + \frac{4F}{3} \right) \frac{\partial^2 \theta}{\partial \eta^2} \quad (28)$$

$$\frac{\partial \phi}{\partial t} - 4 \frac{\partial \phi}{\partial \eta} = \frac{4}{Sc} \frac{\partial^2 \phi}{\partial \eta^2} \quad (29)$$

The corresponding boundary condition (23) in non-dimensional form is

$$\left. \begin{aligned} t \leq 0: & \quad u=0, w=0, \theta=0, \phi=0 \text{ for all } \eta \\ t > 0: & \quad \begin{cases} u=0, w=0, \theta=t, \phi=1 \text{ at } \eta=0 \\ u \rightarrow 0, w \rightarrow 0, \theta \rightarrow 0, \phi \rightarrow 0 \text{ as } \eta \rightarrow \infty \end{cases} \\ t \leq 1: & \quad \theta=t \text{ at } \eta=0 \\ t > 1: & \quad \begin{cases} \theta=1 \text{ at } \eta=0 \\ \theta \rightarrow 0, \phi \rightarrow 0 \text{ as } \eta \rightarrow \infty \end{cases} \end{aligned} \right\} \quad (30)$$

For practical engineering applications and the design of chemical engineering systems, the values of interest include the skin friction coefficient, the couple stress coefficient, the Nusselt number, and the Sherwood number. The local skin friction coefficient, which signifies surface shear stress, is defined as

$$C_f = \frac{\tau_w}{\rho u_w^2}, \tau_w = \left[\mu \frac{\partial u'}{\partial y'} \right]_{y'=0} = \rho V_0^2 u'(0) = \left[\frac{\partial u}{\partial \eta} \right]_{\eta=0} \quad (31)$$

The couple stress coefficient on a wall is given by

$$C_w = \frac{\tau_w}{\rho u_w^2}, w_w = \left[\mu \frac{\partial w'}{\partial y'} \right]_{y'=0} = \rho V_0^2 w'(0) = \left[\frac{\partial w}{\partial \eta} \right]_{\eta=0} \quad (32)$$

The local Nusselt number embodies the ratio of convective to conductive heat transfer across (normal to) a boundary and is a quantification of surface temperature gradient (heat transfer rate on a wall). It is defined as

$$N_u(x') = - \left[\frac{x'}{(T'_w - T'_\infty)} \frac{\partial T'}{\partial y'} \right]_{y'=0} \quad \text{then}$$

$$Nu = \frac{N_u(x')}{R_{e_x}} = - \left[\frac{\partial \theta}{\partial \eta} \right]_{\eta=0} \quad (33)$$

Finally, the local Sherwood number, which encapsulates the ratio of convective to diffusive mass transport and simulates the surface mass transfer rate, is defined thus

$$S_h(x') = - \left[\frac{x'}{(C'_w - C'_\infty)} \frac{\partial C'}{\partial y'} \right]_{y'=0}$$

then $Sh = \frac{S_h(x')}{R_{e_x}} = - \left[\frac{\partial \phi}{\partial \eta} \right]_{\eta=0} \quad (34)$

where $R_{e_x} = - \frac{V_0 x'}{\nu}$.

3. Solution Method

3.1. Numerical solution via the finite element method

The finite element method was implemented to obtain numerical solutions (25) to (28) under boundary condition (29). This technique is extremely efficient and generates robust solutions to complex coupled, nonlinear, multiple-degree differential equation systems. The fundamental steps of the method are summarized below. An excellent description of finite element formulations was also provided by Bathe [40] and Reddy [41].

3.1.1 Step 1: Discretization of a domain into elements

An entire domain is divided into a finite number of sub-domains—a process known as the discretization of the domain. Each sub-domain is termed a “finite element,” and a collection of elements is designated as the “finite element mesh.”

3.1.2. Step 2: Derivation of the elements

The derivation of a finite element (i.e., the

algebraic expressions among the unknown parameters of finite element approximation) involves the following steps:

- a. Construct the variational formulation of the differential equation.
- b. Assume the form of the approximate solution over a typical finite element.
- c. Derive the finite element by substituting the approximate solution into the variational formulation.

These steps result in a matrix equation of the form $[K^e]\{u^e\} = \{F^e\}$, which defines the finite element model of the original equation.

3.1.3. Step 3: Assembly of elements

The algebraic so obtained is assembled by imposing "inter-element" continuity conditions. This assembly yields a large number of algebraic that constitute a global finite element model, which governs the entire flow in the domain.

3.1.4. Step 4: Imposition of boundary conditions

The physical boundary conditions defined in (29) are imposed on the assembled algebraic.

3.1.5. Step 5: Solution of assembled elements

The final matrix equation can be solved through a direct or indirect (iterative) method. For computational purposes, coordinate η is varied from 0 to $\eta_{\max} = 10$, where η_{\max} represents infinity (i.e., external to the momentum, energy, and concentration boundary layers). The entire domain is divided into a set of 100 line segments of equal width (0.1), with each element being two-noded.

3.1.6. Step 6: Variational formulation

The variational formulation associated with (25) to (28) over a typical two-noded linear element (η_e, η_{e+1}) is given by

$$\int_{\eta_e}^{\eta_{e+1}} w_1 \left[\frac{\partial u}{\partial t} - 4 \left(\frac{\partial u}{\partial \eta} \right) - 4 \left(\frac{\partial^2 u}{\partial \eta^2} \right) + Z_1 u \right. \\ \left. + Bmw - (Gr)\theta - (Gc)\phi \right] d\eta = 0 \quad (35)$$

$$\int_{\eta_e}^{\eta_{e+1}} w_2 \left[\frac{\partial w}{\partial t} - 4 \left(\frac{\partial w}{\partial \eta} \right) - 4 \left(\frac{\partial^2 w}{\partial \eta^2} \right) \right. \\ \left. - Z_2 w + Bmu \right] d\eta = 0 \quad (36)$$

$$\int_{\eta_e}^{\eta_{e+1}} w_3 \left[\frac{\partial \theta}{\partial t} - 4 \left(\frac{\partial \theta}{\partial \eta} \right) - \frac{4}{Pr} \left(1 + \frac{4F}{3} \right) \left(\frac{\partial^2 \theta}{\partial \eta^2} \right) \right] d\eta = 0 \quad (37)$$

$$\int_{\eta_e}^{\eta_{e+1}} w_4 \left[\frac{\partial \phi}{\partial t} - 4 \left(\frac{\partial \phi}{\partial \eta} \right) - \frac{4}{Sc} \left(\frac{\partial^2 \phi}{\partial \eta^2} \right) \right] d\eta = 0 \quad (38)$$

where $B = \frac{M}{1+m^2}$, $Z_1 = B + \frac{1}{K}$, $Z_2 = B - \frac{1}{K}$, and

w_1, w_2, w_3 , and w_4 are arbitrary test functions that may be viewed as variations in u, w, θ , and ϕ , respectively. After reducing the order of integration and nonlinearity, we arrive at the following system of equations:

$$\int_{\eta_e}^{\eta_{e+1}} \left[\begin{aligned} & (w_1) \left(\frac{\partial u}{\partial t} \right) - 4(w_1) \left(\frac{\partial u}{\partial \eta} \right) \\ & - 4 \left(\frac{\partial w_1}{\partial \eta} \right) \left(\frac{\partial u}{\partial \eta} \right) + Z_1(w_1)u + Bmw(w_1) \\ & - (Gr)(w_1)\theta - (Gc)(w_1)\phi \end{aligned} \right] d\eta \quad (39)$$

$$- \left[(w_1) \left(\frac{\partial u}{\partial \eta} \right) \right]_{\eta_e}^{\eta_{e+1}} = 0$$

$$\int_{\eta_e}^{\eta_{e+1}} \left[\begin{aligned} & (w_2) \left(\frac{\partial w}{\partial t} \right) - 4(w_2) \left(\frac{\partial w}{\partial \eta} \right) - 4 \left(\frac{\partial w_2}{\partial \eta} \right) \left(\frac{\partial w}{\partial \eta} \right) \\ & - Z_2 w(w_2) + Bmu(w_2) \end{aligned} \right] d\eta \quad (40)$$

$$- \left[(w_2) \left(\frac{\partial w}{\partial \eta} \right) \right]_{\eta_e}^{\eta_{e+1}} = 0$$

$$\int_{\eta_e}^{\eta_{e+1}} \left[\begin{aligned} & (w_3) \left(\frac{\partial \theta}{\partial t} \right) - 4(w_3) \left(\frac{\partial \theta}{\partial \eta} \right) \\ & - \frac{4}{Pr} \left(1 + \frac{4F}{3} \right) \left(\frac{\partial w_3}{\partial \eta} \right) \left(\frac{\partial \theta}{\partial \eta} \right) \end{aligned} \right] d\eta \quad (41)$$

$$- \left[\left(1 + \frac{4F}{3} \right) \left(\frac{w_3}{Pr} \right) \left(\frac{\partial \theta}{\partial \eta} \right) \right]_{\eta_e}^{\eta_{e+1}} = 0$$

$$\int_{\eta_e}^{\eta_{e+1}} \left[\begin{aligned} & (w_4) \left(\frac{\partial \phi}{\partial t} \right) - 4(w_4) \left(\frac{\partial \phi}{\partial \eta} \right) \\ & - \frac{4}{Sc} \left(\frac{\partial w_4}{\partial \eta} \right) \left(\frac{\partial \phi}{\partial \eta} \right) \end{aligned} \right] d\eta \quad (42)$$

$$- \left[\left(\frac{w_4}{Sc} \right) \left(\frac{\partial \phi}{\partial \eta} \right) \right]_{\eta_e}^{\eta_{e+1}} = 0$$

3.1.7. Step 7: Finite element formulation

The finite element model may be obtained on the basis of Eqs. (38) to (41), in which finite element approximations of the following form are substituted

$$u = \sum_{j=1}^2 u_j^e \psi_j^e, w = \sum_{j=1}^2 w_j^e \psi_j^e, \theta = \sum_{j=1}^2 \theta_j^e \psi_j^e, \phi = \sum_{j=1}^2 \phi_j^e \psi_j^e, \tag{43}$$

with $w_1 = w_2 = w_3 = w_4 = \psi_i^e$ ($i = 1, 2$), where u_j^e, w_j^e, θ_j^e , and ϕ_j^e are the primary velocity, secondary velocity, temperature, and concentration, respectively, at the j th node of the typical e th element (η_e, η_{e+1}) . Here, ψ_i^e represents the shape functions of (η_e, η_{e+1}) and are taken as

$$\psi_1^e = \frac{\eta_{e+1} - \eta}{\eta_{e+1} - \eta_e} \text{ and } \psi_2^e = \frac{\eta - \eta_e}{\eta_{e+1} - \eta_e}, \eta_e \leq \eta \leq \eta_{e+1} \tag{44}$$

The finite element model of the e th element thus formed is given by

$$\begin{bmatrix} [K^{11}] \\ [K^{21}] \\ [K^{31}] \\ [K^{41}] \end{bmatrix} \begin{bmatrix} [K^{12}] \\ [K^{22}] \\ [K^{32}] \\ [K^{42}] \end{bmatrix} \begin{bmatrix} [K^{13}] \\ [K^{23}] \\ [K^{33}] \\ [K^{43}] \end{bmatrix} \begin{bmatrix} [K^{14}] \\ [K^{24}] \\ [K^{34}] \\ [K^{44}] \end{bmatrix} \begin{Bmatrix} \{u^e\} \\ \{w^e\} \\ \{\theta^e\} \\ \{\phi^e\} \end{Bmatrix} + \begin{bmatrix} [M^{11}] \\ [M^{21}] \\ [M^{31}] \\ [M^{41}] \end{bmatrix} \begin{bmatrix} [M^{12}] \\ [M^{22}] \\ [M^{32}] \\ [M^{42}] \end{bmatrix} \begin{bmatrix} [M^{13}] \\ [M^{23}] \\ [M^{33}] \\ [M^{43}] \end{bmatrix} \begin{bmatrix} [M^{14}] \\ [M^{24}] \\ [M^{34}] \\ [M^{44}] \end{bmatrix} \begin{Bmatrix} \{u^e\} \\ \{w^e\} \\ \{\theta^e\} \\ \{\phi^e\} \end{Bmatrix} = \begin{Bmatrix} \{b^{1e}\} \\ \{b^{2e}\} \\ \{b^{3e}\} \\ \{b^{4e}\} \end{Bmatrix} \tag{45}$$

where $\{[K^{mn}]\}, [M^{mn}]$ and $\{\{u^e\}, \{w^e\}, \{\theta^e\}, \{\phi^e\}, \{u^e\}, \{w^e\}, \{\theta^e\}, \{\phi^e\} \text{ and } \{b^{me}\}\}$ ($m, n = 1, 2, 3, 4$) are

the set of matrices of orders 4×4 and 4×1 , respectively, and the $'$ (dash) indicates $\frac{d}{d\eta}$. These matrices are defined as follows:

$$\begin{aligned} K_{ij}^{11} &= -4 \int_{\eta_e}^{\eta_{e+1}} \left[(\psi_i^e) \left(\frac{\partial \psi_j^e}{\partial \eta} \right) \right] d\eta \\ &- 4 \int_{\eta_e}^{\eta_{e+1}} \left[\left(\frac{\partial \psi_i^e}{\partial \eta} \right) \left(\frac{\partial \psi_j^e}{\partial \eta} \right) \right] d\eta \\ &+ Z_1 \int_{\eta_e}^{\eta_{e+1}} [(\psi_i^e)(\psi_j^e)] d\eta, \\ K_{ij}^{12} &= Bmw \int_{\eta_e}^{\eta_{e+1}} (\psi_i^e) d\eta \\ K_{ij}^{13} &= -[Gr + Gc] \int_{\eta_e}^{\eta_{e+1}} (\psi_i^e)(\psi_j^e) d\eta, \\ M_{ij}^{11} &= \int_{\eta_e}^{\eta_{e+1}} (\psi_i^e)(\psi_j^e) d\eta, K_{ij}^{21} = K_{ij}^{24} = 0, \\ K_{ij}^{14} &= M_{ij}^{12} = M_{ij}^{13} = M_{ij}^{14} = 0, \\ K_{ij}^{23} &= -Bm \int_{\eta_e}^{\eta_{e+1}} [(\psi_i^e)(\psi_j^e)] d\eta, \\ M_{ij}^{21} &= M_{ij}^{23} = M_{ij}^{24} = 0, M_{ij}^{31} = M_{ij}^{32} = M_{ij}^{34} = 0, \\ M_{ij}^{22} &= \int_{\eta_e}^{\eta_{e+1}} (\psi_i^e)(\psi_j^e) d\eta, K_{ij}^{31} = K_{ij}^{33} = K_{ij}^{34} = 0, \\ M_{ij}^{33} &= \int_{\eta_e}^{\eta_{e+1}} (\psi_i^e)(\psi_j^e) d\eta, K_{ij}^{41} = K_{ij}^{42} = K_{ij}^{43} = 0, \\ K_{ij}^{32} &= -4 \int_{\eta_e}^{\eta_{e+1}} \left[(\psi_i^e) \left(\frac{\partial \psi_j^e}{\partial \eta} \right) \right] d\eta \\ &- \frac{4}{Pr} \left(1 + \frac{4F}{3} \right) \int_{\eta_e}^{\eta_{e+1}} \left[\left(\frac{\partial \psi_i^e}{\partial \eta} \right) \left(\frac{\partial \psi_j^e}{\partial \eta} \right) \right] d\eta, \\ b_i^{2e} &= \left[(\psi_i^e) \left(\frac{\partial w}{\partial \eta} \right) \right]_{\eta_e}^{\eta_{e+1}}, M_{ij}^{31} = M_{ij}^{32} = M_{ij}^{34} = 0, \\ K_{ij}^{22} &= -4 \int_{\eta_e}^{\eta_{e+1}} \left[(\psi_i^e) \left(\frac{\partial \psi_j^e}{\partial \eta} \right) \right] d\eta \\ &- 4 \int_{\eta_e}^{\eta_{e+1}} \left[\left(\frac{\partial \psi_i^e}{\partial \eta} \right) \left(\frac{\partial \psi_j^e}{\partial \eta} \right) \right] d\eta \\ &- Z_2 \int_{\eta_e}^{\eta_{e+1}} [(\psi_i^e)(\psi_j^e)] d\eta, \\ M_{ij}^{44} &= \int_{\eta_e}^{\eta_{e+1}} (\psi_i^e)(\psi_j^e) d\eta, b_i^{1e} = \left[(\psi_i^e) \left(\frac{\partial u}{\partial \eta} \right) \right]_{\eta_e}^{\eta_{e+1}}, \end{aligned}$$

$$b_i^{3e} = \left[\left(\frac{\psi_i^e}{Pr} \right) \left(1 + \frac{4}{3F} \right) \left(\frac{\partial \theta}{\partial \eta} \right) \right]_{\eta_e}^{\eta_{e+1}},$$

$$b_i^{4e} = \left[\left(\frac{\psi_i^e}{Sc} \right) \left(\frac{\partial \phi}{\partial \eta} \right) \right]_{\eta_e}^{\eta_{e+1}}$$

The entire domain is divided into a set of 100 intervals of equal length (0.1). At each node, two functions are to be evaluated. The assembly of the elements therefore produces a set of 123. Given that the system derived after the assembly are nonlinear, an iterative scheme is employed to solve the matrix system. Specifically, the Gauss elimination method is used, thereby maintaining an accuracy of 0.0005.

3.2. Analytical solution via perturbation technique

To find the solution of the system of partial differential equations (25) to (28) in the neighborhood of the plate under condition (29), we assume a perturbation of the forms

$$u(\eta, t) = u_0(\eta) + \frac{\varepsilon}{2} [e^{int} u_1(\eta) + e^{-int} u_2(\eta)] \quad (46)$$

$$w(\eta, t) = w_0(\eta) + \frac{\varepsilon}{2} [e^{int} w_1(\eta) + e^{-int} w_2(\eta)] \quad (47)$$

$$\theta(\eta, t) = \theta_0(\eta) + \frac{\varepsilon}{2} [e^{int} \theta_1(\eta) + e^{-int} \theta_2(\eta)] \quad (48)$$

$$\phi(\eta, t) = \phi_0(\eta) + \frac{\varepsilon}{2} [e^{int} \phi_1(\eta) + e^{-int} \phi_2(\eta)] \quad (49)$$

From Eqs. (45) to (48), we derive

$$\frac{\partial u}{\partial \eta} = u'_o + \frac{\varepsilon}{2} [e^{int} u'_1 + e^{-int} u'_2] \quad (50)$$

$$\frac{\partial^2 u}{\partial \eta^2} = u''_o + \frac{\varepsilon}{2} [e^{int} u''_1 + e^{-int} u''_2] \quad (51)$$

$$\frac{\partial u}{\partial t} = \frac{\varepsilon}{2} [(in)e^{int} u_1 - (in)e^{-int} u_2] \quad (52)$$

$$\frac{\partial w}{\partial \eta} = w'_o + \frac{\varepsilon}{2} [e^{int} w'_1 + e^{-int} w'_2] \quad (53)$$

$$\frac{\partial^2 w}{\partial \eta^2} = w''_o + \frac{\varepsilon}{2} [e^{int} w''_1 + e^{-int} w''_2] \quad (54)$$

$$\frac{\partial w}{\partial t} = \frac{\varepsilon}{2} [(in)e^{int} w_1 - (in)e^{-int} w_2] \quad (55)$$

$$\frac{\partial \theta}{\partial \eta} = \theta'_o + \frac{\varepsilon}{2} [e^{int} \theta'_1 + e^{-int} \theta'_2] \quad (56)$$

$$\frac{\partial^2 \theta}{\partial \eta^2} = \theta''_o + \frac{\varepsilon}{2} [e^{int} \theta''_1 + e^{-int} \theta''_2] \quad (57)$$

$$\frac{\partial \theta}{\partial t} = \frac{\varepsilon}{2} [(in)e^{int} \theta_1 - (in)e^{-int} \theta_2] \quad (58)$$

$$\frac{\partial \phi}{\partial \eta} = \phi'_o + \frac{\varepsilon}{2} [e^{int} \phi'_1 + e^{-int} \phi'_2] \quad (59)$$

$$\frac{\partial^2 \phi}{\partial \eta^2} = \phi''_o + \frac{\varepsilon}{2} [e^{int} \phi''_1 + e^{-int} \phi''_2] \quad (60)$$

$$\frac{\partial \phi}{\partial t} = \frac{\varepsilon}{2} [(in)e^{int} \phi_1 - (in)e^{-int} \phi_2] \quad (61)$$

Substituting Eqs. (45) to (60) into Eqs. (25) to (28), equating harmonic and non-harmonic terms, and disregarding the higher-order terms of $O(\varepsilon^2)$ yield the following set of equations:

$$4u''_o + 4u'_o - Zu_o + Gr\theta_o + Gc\phi_o - Bmw_o = 0 \quad (62)$$

$$4w''_o + 4w'_o - Z_1w_o - Bmu_o = 0 \quad (63)$$

$$\theta''_o + 4Pr\theta'_o - F\theta_o = 0 \quad (64)$$

$$\phi''_o + 4Sc\phi'_o = 0 \quad (65)$$

$$4u''_1 + 4u'_1 - Z_2u_1 + Gr\theta_1 + Gc\phi_1 - Bmw_1 = 0 \quad (66)$$

$$4w''_1 + 4w'_1 + Z_3w_1 - Bmu_1 = 0 \quad (67)$$

$$\theta''_1 + 4Pr\theta'_1 - X_1\theta_1 = 0 \quad (68)$$

$$\phi''_1 + 4Sc\phi'_1 = -inSc\phi_1 = 0 \quad (69)$$

$$4u''_2 + 4u'_2 - Z_2u_2 + Gr\theta_2 + Gc\phi_2 - Bmw_2 = 0 \quad (70)$$

$$4w''_2 + 4w'_2 + Z_4w_2 - Bmu_2 = 0 \quad (71)$$

$$\theta''_2 + 4Pr\theta'_2 + X_2\theta_2 = 0 \quad (72)$$

$$\phi''_2 + 4Sc\phi'_2 + inSc\phi_2 = 0 \quad (73)$$

where the prime denotes differentiation with respect to η and $B = \frac{M}{1+m^2}$, $Z = B + \frac{1}{K}$,

$$Z_1 = B - \frac{1}{K}, \quad Z_2 = Z - in, \quad Z_3 = Z_1 - in,$$

$$Z_4 = Z_1 + in, \quad X_1 = inPr + F, \quad X_2 = inPr - F.$$

The corresponding boundary conditions can be written as follows:

Case 1: Isothermal temperature

$$\left. \begin{aligned}
 &u_o = 0, u_1 = 0, u_2 = 0, w_o = 0, w_1 = 0, w_2 = 0, \\
 &\theta_o = 1, \theta_1 = 1, \theta_2 = 1, \phi_o = 1, \phi_1 = 0, \phi_2 = 0 \\
 &\text{at } \eta = 0 \\
 &u_o = 0, u_1 = 0, u_2 = 0, w_o = 0, w_1 = 0, w_2 = 0, \\
 &\theta_o = 0, \theta_1 = 0, \theta_2 = 0, \phi_o = 0, \phi_1 = 0, \phi_2 = 0 \\
 &\text{as } \eta \rightarrow \infty
 \end{aligned} \right\} \tag{74}$$

Case 2: Ramped temperature

$$\left. \begin{aligned}
 &u_o = 0, u_1 = 0, u_2 = 0, w_o = 0, w_1 = 0, w_2 = 0, \\
 &\theta_o = 0, \theta_1 = 0, \theta_2 = 0, \phi_o = 1, \phi_1 = 0, \phi_2 = 0 \\
 &\text{at } \eta = 0 \\
 &u_o = 0, u_1 = 0, u_2 = 0, w_o = 0, w_1 = 0, w_2 = 0, \\
 &\theta_o = 0, \theta_1 = 0, \theta_2 = 0, \phi_o = 0, \phi_1 = 0, \phi_2 = 0 \\
 &\text{as } \eta \rightarrow \infty
 \end{aligned} \right\} \tag{75}$$

Solving Eqs. (61) to (72) using boundary conditions (74) and (75) yields the expressions for primary and secondary velocities, temperature, and concentration. We obtained a comprehensive range of solutions to the converted conservation equations. To test the validity of the numerical finite element computations, we compared the local skin friction and couple stress coefficients and the Nusselt and Sherwood numbers in Tables 1 to 3 with the solutions obtained using the perturbation technique. The tables show that the results are in excellent agreement. As the numerical solutions are highly accurate, the values of $u, w, \theta,$ and ϕ that correspond to the analytical and numerical solutions are very close to one another.

Table 1: Comparison of local skin friction coefficient and couple stress coefficient with $Gr = 6.0, Gc = 5.0, Pr = 0.71, F = 0.5, Sc = 0.6,$ and $t = 0.5$

Hall parameter	Finite element method	
	Local skin friction coefficient	Couple stress coefficient
0.5	2.325756798	3.023157864
1.0	2.456947862	3.146408538
1.5	2.588279843	3.269659212
2.0	2.717853215	3.392909882
Hall parameter	Perturbation technique	
	Local skin friction coefficient	Couple stress coefficient

	2.3257567990	3.02315786301
0.5	2.4569478630	3.14640853700
1.0	2.5882798440	3.2696592110
1.5	2.7178532160	3.39290988101

3.3. Accuracy of analytical and numerical solutions

Table 2: Comparison of local Nusselt number with $Gr = 5.0, Gc = 5.0, Pr = 0.71, m = 0.5, Sc = 0.6,$ and $t = 0.5$

Radiation number	Finite element method	Perturbation technique
2.0	0.349673412	0.3496734130
1.5	0.407029841	0.4070298420
1.0	0.464386268	0.46438626900
0.5	0.521746697	0.5217466980

Table 3: Comparison of local Sherwood number with $Gr = 6.0, Gc = 5.0, Pr = 0.71, F = 0.5, m = 0.5,$ and $t = 0.5$

Schmidt number	Finite element method	Perturbation technique
0.22	0.4348793152	0.4348793152
0.30	0.4237549217	0.4237549217
0.60	0.419679342	0.412679342
0.78	0.391582079	0.401582079

Table 4: Comparison of current local Sherwood number (Sh) values with the results of Sharma and Chaudhary [37]

	Analytical results of Sharma and Chaudhary [37]		
	$Sc = 0.22$	$Sc = 0.30$	$Sc = 0.78$
Sh	0.2200	0.3000	0.7800
	0.0800	0.1200	0.3800
	- 0.1700	- 0.2100	- 0.4100
	- 0.2700	- 0.3500	- 0.8100
	- 0.0800	- 0.1200	0.3900
	0.2100	0.2600	0.4400
	Present numerical results		
	$Sc = 0.22$	$Sc = 0.30$	$Sc = 0.78$
	0.218862	0.295247	0.774285
	0.079562	0.119627	0.376248
	- 0.169821	- 0.209634	- 0.409631
	- 0.269824	- 0.349625	- 0.806431
	- 0.079562	- 0.119627	0.382645
	0.209634	0.259647	0.436921

4. Code Validation

To evaluate the accuracy of the finite element method, we compared the results with accepted datasets of local Sherwood numbers for MHD viscous incompressible fluid flow past a vertical porous plate immersed in porous medium under the presence of the Hall current; this scenario

corresponds to the case computed by Sharma and Chaudhary [37] in the absence of thermal radiation and phase angle, with the authors adopting different Schmidt numbers and keeping other parameters constant. The results of the evaluation are presented in table 4. This favorable comparison lends confidence to the accuracy of the numerical procedure in the current work. The developed code can therefore be used with great confidence in the study of the problem considered in this paper.

5. Results and Discussion

To analyze the effects of the Hall current, thermal buoyancy force, concentration buoyancy force, thermal diffusion, mass diffusion, thermal radiation, and time on the flow field, numerical values of the primary and secondary fluid velocities in the boundary layer region (computed from numerical solutions (38) and (39)) were plotted graphically against boundary layer coordinate η in Figs. 2 to 15 for various values of the Hall current parameter (m), the thermal Grashof number for heat transfer (Gr), the Grashof number for mass transfer (Gc), the Prandtl number (Pr), the Schmidt number (Sc), the thermal radiation parameter (F), and time (t). In the plotting, we set magnetic permeability parameter K to 0.5, Pr to 0.71, and Sc to 0.22.

Figs. 2 to 15 indicate that for both ramped temperature and isothermal plates, primary velocity u and secondary velocity w attain distinctive maximum values near the surface of the plate, after which the values decrease appropriately with increasing boundary layer coordinate η and thereby approach the free stream value. The primary and secondary fluid velocities are also slower in the ramped temperature plate than in the isothermal plate.

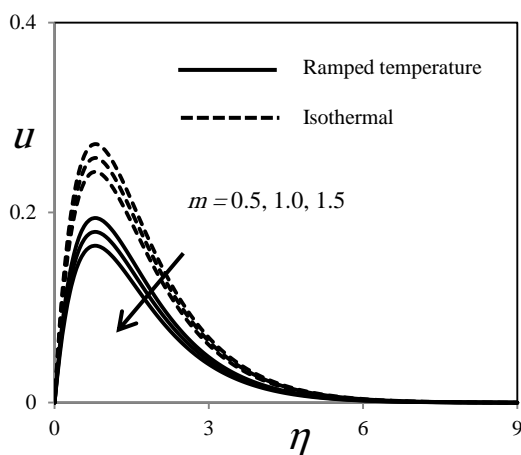


Fig. 2. Primary velocity profiles at $Gr = 6, Gc = 5, Pr = 0.71, Sc = 0.6, F = 5$, and $t = 0.5$.

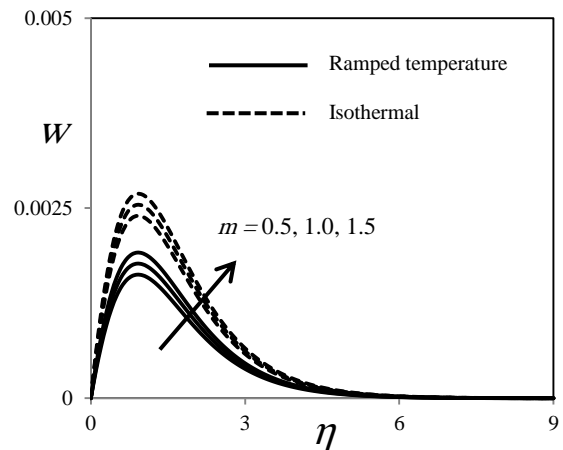


Fig. 3. Secondary velocity profiles at $Gr = 6, Gc = 5, Pr = 0.71, Sc = 0.6, F = 5$, and $t = 0.5$.

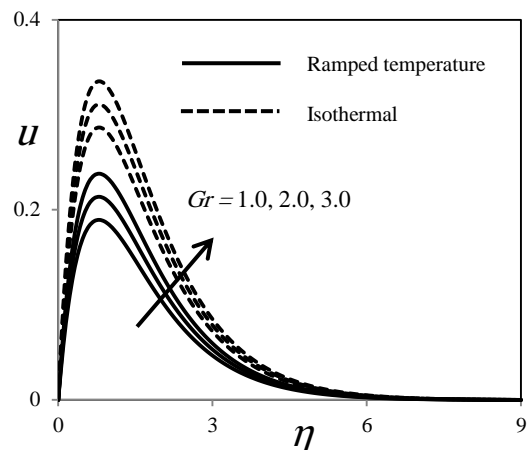


Fig. 4. Primary velocity profiles at $m = 0.5, Gc = 5, Pr = 0.71, Sc = 0.6, F = 5$, and $t = 0.5$.

Fig. 2 illustrates that the primary velocity retards near the plate when Hall parameter m increases. Fig. 3 shows that the secondary velocity increases near the plate and decreases away from the plate with an increase in Hall parameter m . The momentum boundary layer thickness increases with increasing m . The Hall parameter exerts marked effects on the secondary velocity profiles because effective conductivity $\sigma/(1+m^2)$ decreases as m increases. For small values of m , the term $1/(1+m^2)$ decreases, thereby increasing the resistive magnetic force and suppressing the fluid velocity components. This result is a new phenomenon, which emerges as a result of the inclusion of Hall currents. The case $m = 0$ corresponds to the disregard of Hall effects. Moreover, the primary and secondary profiles approach their classical hydrodynamic values when the Hall parameter tends to infinity. This finding is attributed to the fact that the magnetic force terms approach 0 for very large values of the Hall parameter.

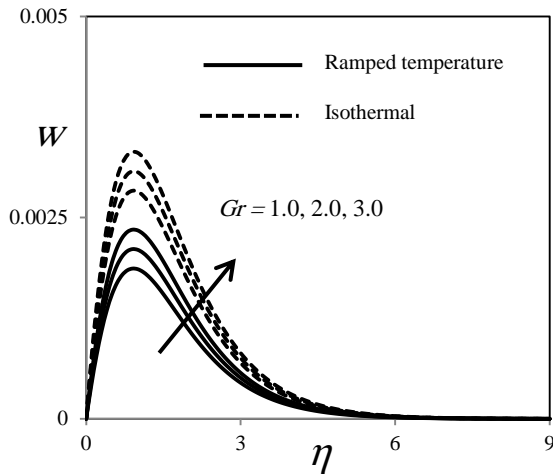


Fig. 5. Secondary velocity profiles at $m = 0.5$, $G_c = 5$, $Pr = 0.71$, $Sc = 0.6$, $F = 5$, and $t = 0.5$.

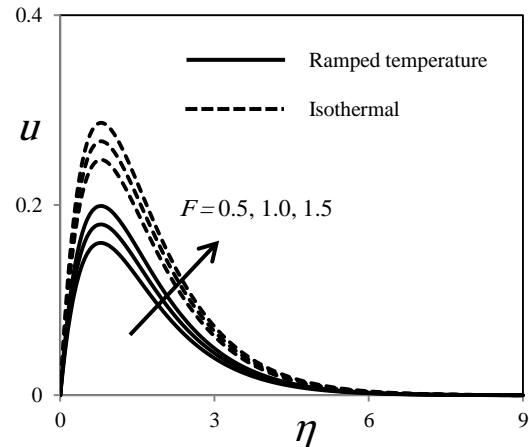


Fig. 8. Primary velocity profiles at $m = 0.5$, $Gr = 6$, $G_c = 5$, $Pr = 0.71$, $Sc = 0.6$, and $t = 0.5$.

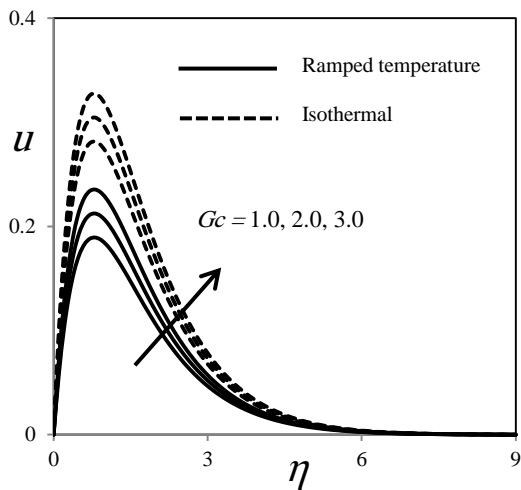


Fig. 6. Primary velocity profiles at $m = 0.5$, $Gr = 6$, $Pr = 0.71$, $Sc = 0.6$, $F = 5$, and $t = 0.5$.

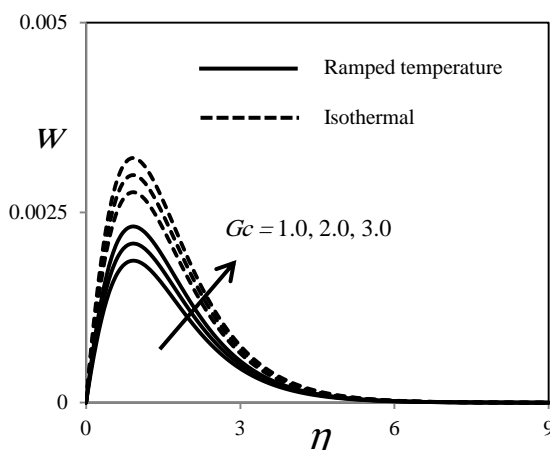


Fig. 7. Secondary velocity profiles at $m = 0.5$, $Gr = 6$, $Pr = 0.71$, $Sc = 0.6$, $F = 5$, and $t = 0.5$.

Figs. 4 to 7 demonstrate the effects of thermal and concentration buoyancy forces on the primary and secondary fluid velocities in the ramped temperature and isothermal plates. In these plates, u and w increase with rising Gr and G_c . Gr represents the strength of thermal buoyancy force relative to viscous force, and G_c represents the strength of concentration buoyancy force relative to viscous force. Therefore, Gr and G_c increase with rising strengths of thermal and concentration buoyancy forces, respectively, relative to viscous force. In this problem, natural convective flow is induced by thermal and concentration buoyancy forces. Correspondingly, the thermal and concentration buoyancy forces tend to accelerate the primary and secondary fluid velocities throughout the boundary layer regions of both the ramped temperature and isothermal plates (Figs. 4–7).

Figs. 8 and 9 indicate that for the ramped temperature and isothermal plates, radiation parameter F tends to accelerate the translational velocity (primary and secondary) and the ramped and isothermal temperatures in the entire boundary layer region. Generally, radiation increases with rising temperature; ultimately, velocity also rises. Figs. 10 and 11 depict the effects of time on fluid flow in the boundary layer regions of the ramped temperature and isothermal plates. The figures show that u and w increase with increasing t in both plates, implying that fluid flow in the boundary layer regions of the plates accelerates with the progression of time. The numerical values of fluid temperature θ , computed from numerical solution (40), are plotted graphically against boundary layer coordinate η in Figs. 12 to 14 for various values of F , Pr , and t . Fig. 12 indicates that fluid temperature θ increases with rising F in both the ramped temperature and isothermal plates. Thus, thermal radiation tends to enhance fluid temperature throughout the boundary layer regions in the plates. Thermal radiation provides an additional means of diffusing energy because thermal radiation

parameter $F = \frac{4\sigma_s T_\infty^3}{k_e \mathcal{K}}$ and, therefore, a Rosseland mean absorption coefficient decrease as F increases at fixed k_e values of T_∞' and \mathcal{K} .

Fig. 13 shows the temperature distribution influenced by the Prandtl number for the ramped and isothermal temperatures. The fluid temperature decreases as the Prandtl number increases in the entire boundary layers of the ramped and isothermal temperatures. Because Pr is the relative strength of viscosity and thermal conductivity of the fluid, this parameter decreases when the thermal conductivity of the fluid increases. This result suggests that thermal diffusion tends to enhance fluid temperature. As time progresses, fluid temperature is enhanced in both the ramped temperature and isothermal plates. Fig. 14 illustrates that the fluid temperature is at its maximum on the surfaces of the ramped temperature and isothermal plates. It decreases with increasing boundary layer coordinate η , thereby approaching the free stream value. Finally, the fluid temperature is lower in the ramped temperature plate than in the isothermal plate.

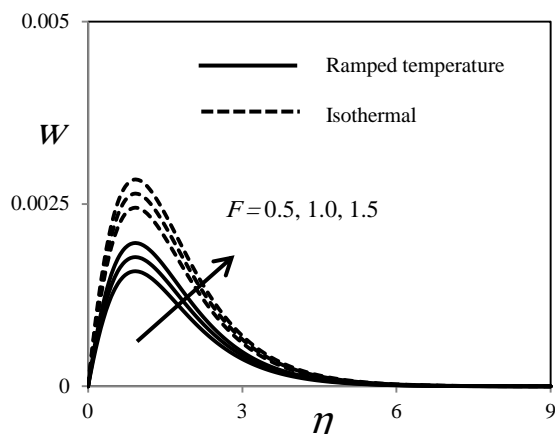


Fig. 9. Secondary velocity profiles at $m = 0.5$, $Gr = 6$, $Gc = 5$, $Pr = 0.71$, $Sc = 0.6$, and $t = 0.5$.

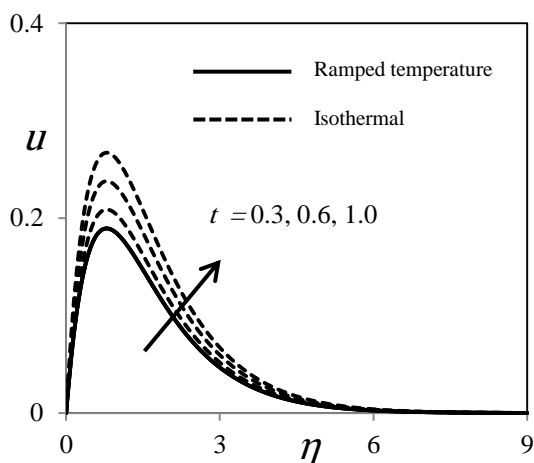


Fig. 10. Primary velocity profiles at $m = 0.5$, $Gr = 6$, $Gc = 5$, $Pr = 0.71$, $Sc = 0.6$, and $F = 5$.

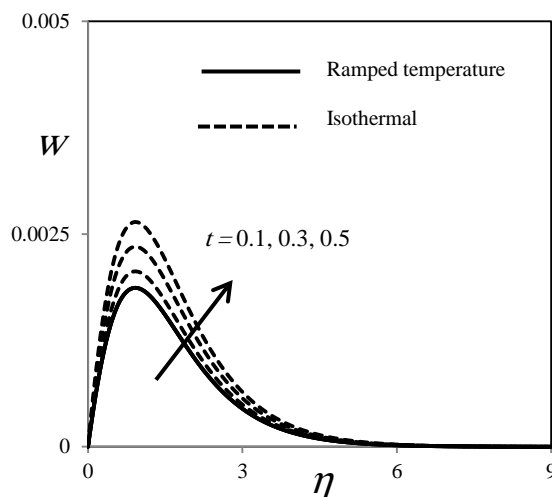


Fig. 11. Secondary velocity profiles at $m = 0.5$, $Gr = 6$, $Gc = 5$, $Pr = 0.71$, $Sc = 0.6$, and $F = 5$.

Fig. 15 presents the effects of mass diffusion on the fluid flow in the boundary layer regions of the ramped temperature and isothermal plates. Fluid concentration ϕ decreases with increasing Sc , which represents the ratio of momentum diffusivity and molecular (mass) diffusivity. Sc decreases with increasing mass diffusivity, implying that mass diffusion tends to accelerate fluid flow in the boundary layer regions of the two plates. We also recorded numerical values of the surface local skin friction coefficients (C_f and C_w) and Nusselt number (Nu) at different values of Gr , Gc , M , m , and F (Tables 5 to 10, respectively) for the isothermal and ramped temperature plates. Tables 5 to 9 indicate that the skin friction coefficients (C_f and C_w) increase with rising Gr , Gc , and m , whereas the reverse effect was observed for C_f and C_w , which improve with increases in M and F in both cases (isothermal and ramped). Table 10 shows that the Nu decreases with increasing F in the ramped temperature and isothermal plates.

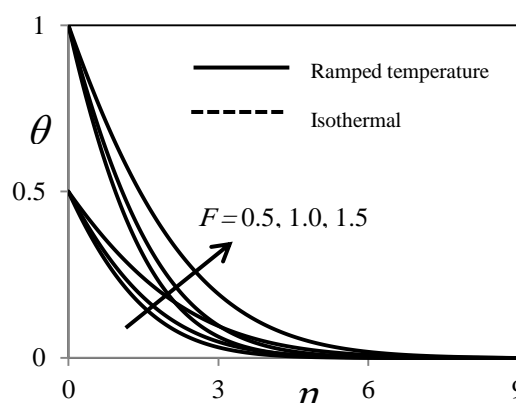


Fig. 12. Temperature profiles at $Pr = 0.71$ and $t = 0.5$.

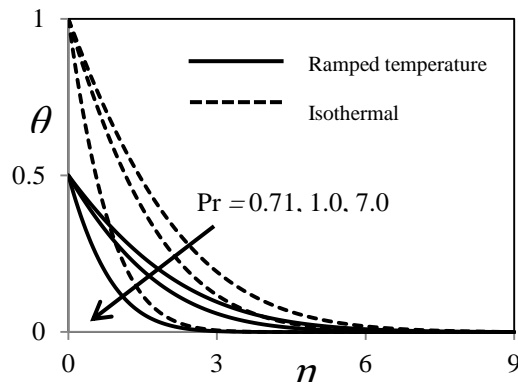


Fig. 13. Temperature profiles at $F = 5$ and $t = 0.5$.

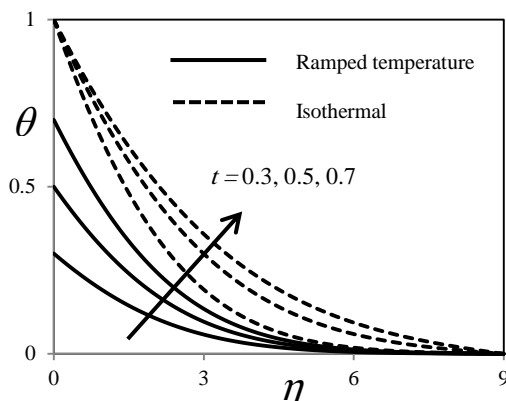


Fig. 14. Temperature profiles at $F = 5$ and $Pr = 0.71$.

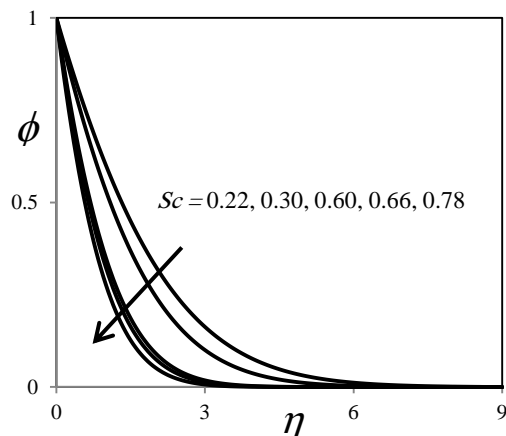


Fig. 15. Concentration profiles at different values of Sc .

Table-5: Effect of Gr on C_f and C_w in case of isothermal and ramped temperatures

Gr	C_f		C_w	
	Isothermal	Ramped	Isothermal	Ramped
1.0	0.4312621	0.4180319	0.0005132	0.0004826
2.0	0.4523194	0.4316692	0.0005316	0.0005055
3.0	0.4702158	0.4520036	0.0005564	0.0005249

Table 6: Effects of Gc on C_f and C_w under isothermal and ramped temperatures

Gc	C_f		C_w	
	Isothermal	Ramped	Isothermal	Ramped
1.0	0.4492615	0.4263189	0.0005248	0.0005048
2.0	0.4629747	0.4418594	0.0005493	0.0005269
3.0	0.4839541	0.4680157	0.0005614	0.0005418

Table 7: Effects of M on C_f and C_w under isothermal and ramped temperatures

M	C_f		C_w	
	Isothermal	Ramped	Isothermal	Ramped
0.5	0.4215862	0.4430815	0.0004056	0.0004231
1.0	0.3954103	0.4013592	0.0003621	0.0003917
1.5	0.3621894	0.3715463	0.0003328	0.0003618

Table 8: Effects of m on C_f and C_w under isothermal and ramped temperatures

m	C_f		C_w	
	Isothermal	Ramped	Isothermal	Ramped
0.5	0.4326557	0.4105331	0.0004132	0.0003926
1.0	0.4413581	0.4296145	0.0004305	0.0004163
1.5	0.4563175	0.4406218	0.0004531	0.0004362

Table 9: Effects of F on C_f and C_w under isothermal and ramped temperatures

F	C_f		C_w	
	Isothermal	Ramped	Isothermal	Ramped
0.5	0.4203462	0.4413644	0.0003952	0.0003715
1.0	0.3918722	0.4015843	0.0003621	0.0003469
1.5	0.3629883	0.3624475	0.0003578	0.0003182

Table 10: Effects of F on Nu under isothermal and ramped temperatures

F	Nu	
	Isothermal ($t = 1.0$)	Ramped temperature ($t = 0.5$)
0.5	0.96254871	0.47526984
1.0	0.92434182	0.44069521
1.5	0.89214413	0.40531899

6. Conclusion

This research work investigated the effects of the Hall current on the unsteady hydromagnetic natural convective flow (with heat and mass transfer) of a viscous, incompressible, electrically conducting, and optically thick radiating fluid past an impulsively moving vertical plate embedded in a fluid-saturated porous medium. The temperature of the plate was temporarily ramped for the analysis. The significant findings for ramped temperature and isothermal plates are summarized as follows.

- The Hall current tends to accelerate the secondary fluid velocity throughout the boundary layer region.
- The primary and secondary fluid velocities accelerate with the progression of time throughout the boundary layer region.
- Thermal radiation and thermal diffusion tend to enhance fluid temperature, and fluid temperature increases over time throughout the boundary layer region.
- The Nusselt number derived on the basis of the temperature profiles decreases with increasing Prandtl number, thermal radiation, and time throughout the boundary layer.
- The Schmidt number and time tend to reduce the Sherwood number throughout the boundary layer.
- The numerical solutions are highly accurate, and the values of the primary and secondary velocities, temperature, and concentration that correspond to the analytical and numerical solutions are very close to one another.

Applications of the research

The problem pursued in this work presents many scientific and engineering applications, including the following:

- a) Analysis of blood flow through arteries
- b) Soil mechanics, water purification, and powder metallurgy
- c) Study of the interaction between a geomagnetic field and a geothermal region
- d) Petroleum engineering applications concerned with the movement of oil, gas, and water through oil or gas reservoirs

6.2. Scope for future research

Future research work can use the finite element method implemented in the current work as it is a very useful approach to solving linear and nonlinear partial and ordinary differential equations in physics, mechanical engineering, and other similar fields. The results obtained are more accurate than those derived using other numerical methods. The finite element approach is currently used by mechanical engineers to solve complex problems.

Nomenclature

List of variables

\vec{B}	Magnetic induction vector
B_o	Intensity of applied magnetic field (<i>Tesla</i>)
C_p	Specific heat at constant pressure, ($J K^{-1} Mole^{-1}$)
\vec{E}	Electric field
e	Electron charge, <i>Coloumb</i>
C'_∞	Concentration in fluid far from plate ($Kg m^{-3}$)
C'	Species concentration of fluid at plate ($Kg m^{-3}$)
C'_w	Concentration of plate ($Kg m^{-3}$)
D	Chemical molecular diffusivity ($m^2 s^{-1}$)
x'	Coordinate axis along plate (m)
y'	Co-ordinate axis normal to plate (m)
u'	Velocity component in x' – direction ($m s^{-1}$)
v'	Velocity component in y' – direction ($m s^{-1}$)
w'	Velocity component in z' – direction ($m s^{-1}$)
Gr	Grashof number for heat transfer
Gc	Grashof number for mass transfer
Pr	Prandtl number
Sc	Schmidt number
p_e	Electron pressure ($N m^{-2}$)
T'	Temperature of fluid (K)
T'_w	Temperature of plate (K)
T'_∞	Fluid temperature far from plate (K)
t	Time (s)
t'	Dimensional time (s)
q_r	Radiative heat transfer coefficient
\vec{J}	Current density vector ($A. s. m^{-2}$)
(J_x, J_y, J_z)	Scalar Components of \vec{J}
u	Velocity component in x' – direction ($m s^{-1}$)
\vec{v}	Velocity vector
V_o	Reference velocity ($m s^{-1}$)
w	Velocity component in z' – direction ($m s^{-1}$)
g	Acceleration due to gravity ($m s^{-2}$)
K	Permeability of porous medium (m^2)
M	Hartmann number
m	Hall parameter
F	Thermal radiation parameter
Nu	Local Nusselt number
Sh	Local Sherwood number
Re_x	Reynolds number
C_f	Local skin friction coefficient due to primary velocity (u)
C_w	Local skin friction coefficient due to

secondary velocity (w)

P Pressure (Pa)

k' Dimensional permeability of porous medium

t_o Characteristic time ((s))

Greek symbols

β Coefficient of volume expansion (K^{-1})

ρ Density of fluid (kg/m^{-3})

β^* Volumetric coefficient of expansion with concentration ($m^3 Kg^{-1}$)

U Kinematic viscosity (m^2s^{-1})

ω_e Electron frequency (Hertz)

τ'_w Shear stress (N/m^2)

θ Dimensionless temperature (K)

ϕ Dimensionless concentration ($Kg m^{-3}$)

σ Electrical conductivity ($\Omega^{-1}m^{-1}$)

τ_e Electron collision time (S)

τ_i Ion collision time (S)

η_e Number of electron density

η Spatial coordinate (m)

ω_i Ion frequency (Hertz)

K Thermal conductivity, W/mK

Superscript

' Dimensionless properties

Subscripts

W Conditions on wall

∞ Free stream conditions

p Plate

References

[1]. R. Srinivasa Raju, G. Jithender Reddy, J. Anand Rao, M. M. Rashidi, Rama Subba Reddy Gorla, "Analytical and Numerical Study of Unsteady MHD Free Convection Flow over an Exponentially Moving Vertical Plate With Heat Absorption", *Int. J. Thermal Sci.*, 107, 303-315 (2016).
 [2]. S. Reddy Sheri, R. Srinivasa Raju, "Transient MHD free convective flow past an infinite vertical plate embedded in a porous medium with viscous dissipation", *Meccanica*, 51(5), 1057-1068, (2016).
 [3]. R. Srinivasa Raju, B. Mahesh Reddy, M.M. Rashidi, Rama Subba Reddy Gorla, "Application of Finite Element Method to Unsteady MHD Free Convection Flow Past a Vertically Inclined Porous Plate Including Thermal

Diffusion And Diffusion Thermo Effects", *J. Porous Media*, 19 (8), 701-722, (2016).

[4]. R. Srinivasa Raju, G. Jithender Reddy, J. Anand Rao, M.M. Rashidi, "Thermal Diffusion and Diffusion Thermo Effects on an Unsteady Heat and Mass Transfer MHD Natural Convection Couette Flow Using FEM", *J. Comp. Design and Eng.*, 3 (4), 349-362, (2016).

[5]. M.V. Ramana Murthy, R. Srinivasa Raju, J. Anand Rao, "Heat and Mass transfer effects on MHD natural convective flow past an infinite vertical porous plate with thermal radiation and Hall Current", *Procedia Eng. J.*, 127, 1330-1337, (2015).

[6]. S. Sivaiah, R. Srinivasa Raju, "Finite Element Solution of Heat and Mass transfer flow with Hall Current, heat source and viscous dissipation", *Appl. Math. Mech.*, 34 (5), 559-570, (2013).

[7]. J. Anand Rao, R. Srinivasa Raju, S. Sivaiah, "Finite Element Solution of heat and mass transfer in MHD Flow of a viscous fluid past a vertical plate under oscillatory suction velocity", *J. Appl. Fluid Mech.*, 5 (3), 1-10, (2012).

[8]. J. Anand Rao, S. Sivaiah, R. Srinivasa Raju, "Chemical Reaction effects on an unsteady MHD free convection fluid flow past a semi-infinite vertical plate embedded in a porous medium with Heat Absorption", *J. Appl. Fluid Mech.*, 5 (3), 63-70, (2012).

[9]. G. Jithender Reddy, R. Srinivasa Raju, J. Anand Rao, "Thermal Diffusion and Diffusion Thermo impact on Chemical reacted MHD Free Convection from an Impulsively Started Infinite Vertical Plate embedded in a Porous Medium using FEM", *J. Porous Media*, 20 (12), 1097-1117, (2017).

[10]. R. Dodda, R. Srinivasa Raju, J. Anand Rao, "Influence Of Chemical Reaction On MHD boundary Layer flow Of Nano Fluids Over A Nonlinear Stretching Sheet With Thermal Radiation", *J. Nanofluids*, 5 (6), 880-888, (2016).

[11]. R. Dodda, R. Srinivasa Raju, J. Anand Rao, "Slip Effect of MHD Boundary Layer Flow of Nanofluid Particles over a Nonlinearly Isothermal Stretching Sheet in Presence of Heat Generation/Absorption", *Int. J. Nanosci. Nanotech.*, 12(4), 251-268, (2016).

[12]. J. Anand Rao, R. Srinivasa Raju, S. Sivaiah, "Finite Element Solution of MHD transient flow past an impulsively started infinite horizontal porous plate in a rotating fluid with Hall current", *J. Appl. Fluid Mech.*, 5(3), 105-112, (2016).

[13]. V.S. Rao, L. Anand Babu, R. Srinivasa Raju, "Finite Element Analysis of Radiation and mass transfer flow past semi-infinite moving vertical plate with viscous dissipation", *J. Appl. Fluid Mech.*, 6 (3), 321-329, (2013).

[14]. R. Srinivasa Raju, "Combined influence of thermal diffusion and diffusion thermo on unsteady hydromagnetic free convective fluid flow past an infinite vertical porous plate in presence of chemical reaction", *J. Inst. Eng.: Series C*, 97(4), 505-515, (2016).

[15]. R. Srinivasa Raju, K. Sudhakar, M. Rangamma, "The effects of thermal radiation and Heat source on an unsteady

- MHD free convection flow past an infinite vertical plate with thermal diffusion and diffusion thermo", *J. Inst. Eng.: Series C*, 94(2), 175-186, (2013).
- [16]. A. Aghaei, H. Khorasanizadeh, G. Sheikhzadeh, Mahmoud Abbaszadeh, "Numerical study of magnetic field on mixed convection and entropy generation of nanofluid in a trapezoidal enclosure", *J. Magn. Mater.*, 403, 133-145, (2016).
- [17]. A. Aghaei, A. A. Abbasian Arani, F. Abedi, "Analysis of Magnetic Field Effects on Distributed Heat Sources in a Nanofluid-Filled Enclosure by Natural Convection", *J. Appl. Fluid Mech.*, 9(3), 1175-1187, (2016).
- [18]. R. Deka, U. N. Das, V. M. Soundalgekar, "Effects of mass transfer flow past an impulsively started infinite vertical plate with constant heat flux and chemical reaction", *Forsch. Ingenieurwes.*, 60, 284-287, (1994).
- [19]. R. Muthucumaraswamy, P. Ganesan, "Effect of the chemical reaction and injection on flow characteristics in an unsteady upward motion of an isothermal plate", *J. Appl. Mech. Tech. Phys.*, 42, 665-671, (2001).
- [20]. A.J. Chamkha, "MHD flow of a uniformly stretched vertical permeable surface in the presence of heat generation/absorption and a chemical reaction", *Int. Commun. Heat Mass Transfer*, 30, 413-422, (2003).
- [21]. F.S. Ibrahim, A.M. Elaiw, A.A. Bakr, "Effect of the chemical reaction and radiation absorption on the unsteady MHD free convection flow past a semi infinite vertical permeable moving plate with heat source and suction", *Commun. Nonlinear Sci. Numer. Simul.*, 13, 1056-1066, (2008).
- [22]. M.M. Rahman, "Convective flows of micropolar fluids from radiate isothermal porous surfaces with viscous dissipation and Joule heating", *Commun. Nonlinear Sci. Numer. Simul.*, 14, 3018-3030, (2009).
- [23]. A.C. Cogley, W.E. Vincenty, S.E. Gilles, "Differential approximation for radiation in a non-gray gas near equilibrium", *AIAA J.*, 6, (1968) pp. 551-553.
- [24]. M.D. Abdus Sattar, Kalim MD. Hamid, "Unsteady free-convection interaction with thermal radiation in a boundary layer flow past a vertical porous plate", *J. Math. Phys. Sci.*, 30, 25-37, (1996).
- [25]. K. Vajravelu, "Flow and heat transfer in a saturated porous medium", *ZAMM*, 74, 605-614, (1994).
- [26]. M.A. Hossain, H.S. Takhar, "Radiation effect on mixed convection along a vertical plate with uniform surface temperature", *Heat Mass Transf.*, 31, 243-248, (1996).
- [27]. A. Raptis, "Radiation and free convection flow through a porous medium", *Int. Commun. Heat Mass Transf.*, 25, 289-295, (1998).
- [28]. O.D. Makinde, "Free convection flow with thermal radiation and mass transfer past a moving vertical porous plate", *Int. Commun. Heat Mass Transf.*, 32, 1411-1419, (2005).
- [29]. F.S. Ibrahim, A.M. Elaiw, A.A. Bakr, "Effect of the chemical reaction and radiation absorption on unsteady MHD mixed convection flow past a semi-infinite vertical permeable moving plate with heat source and suction", *Commun. Nonlinear Sci. Numer. Simul.*, 13, 1056-1066, (2008).
- [30]. A.A. Bakr, "Effects of chemical reaction on MHD free convection and mass transfer flow of a micropolar fluid with oscillatory plate velocity and constant heat source in a rotating frame of reference", *Commun. Nonlinear Sci. Numer. Simul.*, 16, 698-710, (2011).
- [31]. I. Pop, T. Watanabe, "Hall effect on magneto hydrodynamic free convection about a semi-infinite vertical flat plate", *Int. J. Eng. Sci.*, 32, 1903-1911, (1994).
- [32]. E.M. Abo-Eldahab, E.M.E. Elbarbary, "Hall current effect on magnetohydrodynamic free-convection flow past a semi-infinite vertical plate with mass transfer", *Int. J. Eng. Sci.*, 39, 1641-52, (2001).
- [33]. H.S. Takhar, S. Roy, G. Nath, "Unsteady free convection flow over an infinite vertical porous plate due to the combined effects of thermal and mass diffusion, magnetic field and Hall currents", *Heat Mass Transf.*, 39, 8258-34, (2003).
- [34]. L.K. Saha, S. Siddiqua, M.A. Hossain, "Effect of Hall current on MHD natural convection flow from vertical permeable flat plate with uniform surface heat flux", *Appl. Math. Mech. -Engl. Ed.*, 32(9), 1127-1146, (2011).
- [35]. P.V. Satya Narayana B. Venkateswarlu, S. Venkataramana, "Effects of Hall current and radiation absorption on MHD micropolar fluid in a rotating system", *Ain Shams Eng. J.*, <http://dx.doi.org/10.1016/j.asej.2013.02.002>, (2013).
- [36]. G.S. Seth, G.K. Mahato, S. Sarkar, "Effects of Hall current and rotation on MHD natural convection flow past an impulsively moving vertical plate with ramped temperature in the presence of thermal diffusion with heat absorption", *Int. J. Energy Tech.*, 5(16), 1-12, (2013).
- [37]. B.K. Sharma, R.C. Chaudhary, "Hydromagnetic unsteady mixed convection and mass transfer flow past a vertical porous plate immersed in a porous medium with Hall Effect", *Eng. Trans.*, 56(1), 3-23, (2008).
- [38]. K.R. Cramer, S.I. Pai, "Magnetofluid dynamics for engineers and applied physicists", McGraw Hill Book Company, New York (1973).
- [39]. M.Q. Brewster, "Thermal Radiative Transfer and Properties", John Wiley & Sons, New York, USA, (1992).
- [40]. K.J. Bathe, "Finite Element Procedures", Prentice-Hall, New Jersey, (1996).
- [41]. J.N. Reddy, "An Introduction to the Finite Element Method", McGraw-Hill Book Company, New York, 3rd Edition, (2006).

